Tribology Letters, Vol. 18, No. 4, April 2005 (© 2005)
DOI: 10.1007/s11249-005-3610-0

Friction coefficient of soft contact lenses: measurements and modeling

A.C. Rennie, P.L. Dickrell and W.G. Sawyer*
Department of Mechanical and Aerospace Engineering, University of Florida, Gainesville, FL 32611, USA

Received 12 October 2004; accepted 16 January 2005

Tribological conditions for contact lenses have very low contact pressures in the range 3–5 kPa and sliding speeds around 12 cm/s. Using a microtribometer a series of experiments was run on commercially available contact lenses made from Etafilcon-A. These tests were run using 10–50 mN of normal load at speeds from 63 to 6280 μm/s using a 1-mm radius glass sphere as a pin. The resulting contact pressures are believed to be nearly an order of magnitude larger than the targeted 3–5 kPa. It is hypothesized that the viscoelastic nature of the hydrogel, viscous shearing of the packaging solution, and interfacial shear between the glass sphere and the contact lens all contribute to the friction forces. A model that includes all three of these contributors is developed and compared to the experimental data. The experimental friction coefficients vary from μ = 0.025 to 0.075. The calculated fluid film thicknesses were between 1 and 30 nm. The average surface roughness of the lens and the glass sphere are R_a = 15 nm and R_a = 8 nm, respectively, suggesting that the contact is not in full elastohydrodynamic lubrication. Finally, the largest contributors to the friction force in these experiments were found to be viscous dissipation within the hydrogel and interfacial shear within the contact zone.

KEY WORDS: contact lens, hydrogel friction, microtribology, microtribometer

1. Introduction

Hydrogels are polymer matrices that contain 30–70% water [1] and are the primary material for soft contact lenses. Although soft materials are well suited for the eye, a significant fraction of people are unable to wear contact lenses because of extensive eye irritation. There is an existing clinical hypothesis that ocular comfort is related to friction. The mechanical properties of hydrogels are extremely sensitive to water content and humidity, and contact pressure is known to cause redistribution and/or reduction of the water content of hydrogel materials [2]. Therefore, tribological testing of hydrogels must be done under low contact pressure conditions.

Nairn and Jiang [3] reported the friction coefficients of polyhydroxy ethyl methacrylate (p-HEMA) based lenses to be in the range of μ = 0.060–0.115 using a custom-built pin-on-disk tribometer. The contact pressure in their study was 3.5 kPa. Freeman *et al.* [4] reported the friction coefficient of flat disks of p-HEMA hydrogels to be in the range of μ = 0.02–1.7 over a wide range of applied load, lubrication, hydrogel crosslink density, and degree of hydrogel hydration again using a special purpose tribometer.

This study aims to identify the various contributions to friction force in a microtribological contact with a saturated hydrogel. The *in vitro* conditions are selected to come as close as possible to the pressures and speeds experienced *in vivo* using existing microtribometry. Blinking is assumed to be the primary force and motion contribution for contact lens tribology. Estimates of the contact pressure created by the eyelid during blinking range from 3.5 to 4.0 kPa and blinking speed average around 12 cm/s [3,5,6]. This combination of low contact pressure and moderate sliding speed are challenging. In this study a reciprocating microtribometer is used to explore the contact pressure and speed dependence of friction coefficient measurements of contact lenses.

*To whom correspondence should be addressed.
E-mail: wgsawyer@ufl.edu

2. Experimental setup

Tribology experiments were run on a reciprocating microtribometer that uses dual glass flexures to apply mN-range normal loads and react mN-range frictional forces [7]. The tribometer is mounted on an active vibration isolation granite table inside a softwall cleanroom. The apparatus is shown in figure 1. For these experiments commercially available soft contact lenses made from Etafilcon-A [8] were mounted onto plastic base curves that match the internal radius of curvature of the lenses. The pin sample is a borosilicate crown glass sphere of radius 1mm, and the base curves and contact lenses have a radius of curvature of approximately 7.1 mm. Material properties and surface characterization of the samples are given in table 1.

All tests were run using the same experimental procedure: (1) a clean and dry base curve is positioned on

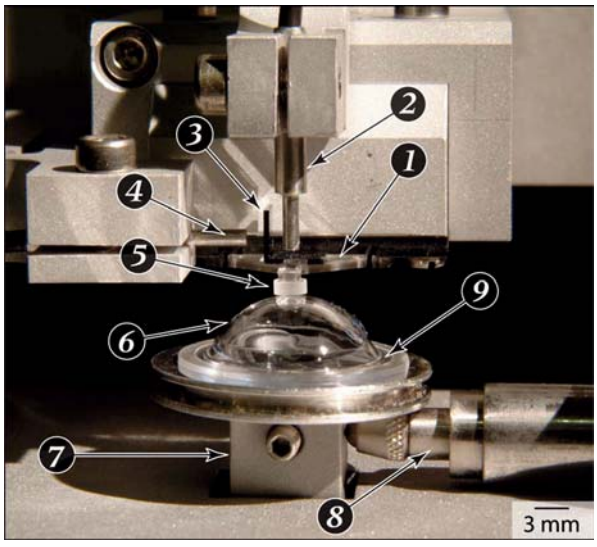

Figure 1. Photograph of the micro-tribometer setup showing: (1) glass flexure to react normal load and friction forces, (2) optical sensor for vertical deflections, (3) mirrors, (4) optical sensor for horizontal deflections, (5) borosilicate crown glass pin with a 7 mm radius of curvature (a) 1-mm radius sphere was used in this study), (6) Etafilcon-A contact lens, (7) reciprocating stage, (8) LVDT for stage position measurements, and (9) plastic base curve used to hold the contact lens.

Table 1.
Material properties of the glass sphere and the Etafilcon-A contact lenses.

		Glass sphere	Contact lens
Average roughness	R_a	8 nm[a]	15 nm[12]
Radius of curvature	R	1 mm[b]	7.1 mm[b]
Elastic modulus	E	60 GPa[b]	255 kPa[b]
Poisson ratio	ν	0.30	0.45[b]
Thickness	c		100 μm[b]

[a]Collected using a scanning white-light interferometer.
[b]Manufacturer reported values.

the microtribometer reciprocating stage, (2) a clean and dry glass sphere is mounted to the glass cantilever, (3) a new contact lens package is opened, (4) the lens is removed from the package by hand (only the back side of the lens is handled), (5) the lens is transferred onto the base curve, (6) final positioning of the lens on the base curve is done with clean stainless steel tweezers, (7) the lens and base curve assembly is positioned under the borosilicate pin near the apex of the curve, (8) a normal load is applied, and (9) the test is initiated and run for a prescribed number of cycles (based on sliding speed). Steps 3–8 are completed in less than 1 min or the test is abandoned. The experimental conditions used in this study are given in table 2.

Table 2.
Experimental conditions.

Applied normal load	F_n	3–20 mN
Reciprocating amplitude		0.60 mm
Reciprocating frequency		0.07–6.66 Hz
Sliding speed	V	63–6280 μm/s
Relative humidity		46–51%
Sampling rate		100 Hz

3. Modeling

The modeling of the experiments done on these contact lenses begins by assuming that the lens can be reasonably modeled with a modified Winkler surface [9]. The modification is the inclusion of a viscous damper into the traditional bed-of-springs elements. This is given by equation (1) where P (Pa) is the contact pressure, E (Pa) is the elastic modulus, ν is Poisson's ratio, c (mm) is the thickness, δ (mm) is the normal deformation, β ((Pa s)/mm) is the viscous coefficient, and $\dot{\delta}$ (mm/s) is the rate of normal deformation. A contact schematic is shown in figure 2.

$$P = \frac{E}{(1-\nu^2)c}\delta + \beta\dot{\delta} = \mathrm{k_s}\delta + \beta\dot{\delta} \qquad (1)$$

The normal load F_n for quasi-static indentation of two spheres can be found by integrating equation (1) over

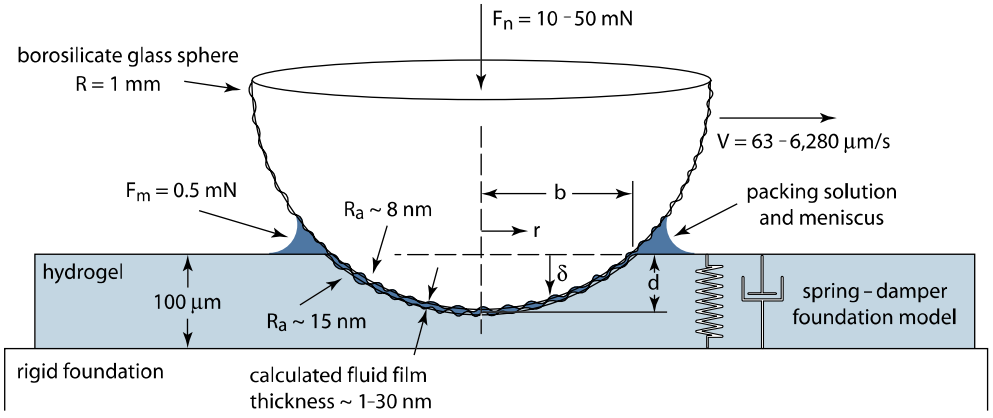

Figure 2. A contact schematic and nomenclature showing the modified Winkler foundation material model. The meniscus, lens thickness, fluid film thickness, surface roughness, and deformation are all exaggerated.

the circular contact of diameter $2b$ in polar coordinates, where r is the radial coordinate going from 0 to b, and θ is the angular coordinate with $\theta = 0$ lying along the direction of travel.

$$F_n = \int_0^{2\pi}\int_0^{b} P\, r dr\, d\theta = k_s \int_0^{2\pi}\int_0^{b} \delta\, r dr\, d\theta \cong k_s \frac{\pi b^4}{4R'} \quad (2)$$

In equation (2), R' is the composite radius of curvature as given by equation (3), where R_1 and R_2 are the radii of curvature of the two spheres. The approach of centers d for this contact is given by equation (4). The relationship between d and F_n requires solving equation (2) for the contact radius and inserting this result into equation (4).

$$\frac{1}{R'} = \frac{1}{R_1} + \frac{1}{R_2} \quad (3)$$

$$d = R_1 + R_2 - \sqrt{R_1^2 - b^2} - \sqrt{R_2^2 - b^2} \quad (4)$$

For the Hertzian contact problem the approach of centers is given by equation (5) [10], where the effective elastic modulus E' is given by equation (6) (the borosilicate glass sphere is assumed to be rigid with respect to the contact lens material).

$$d = \frac{1}{2}\left(\frac{9}{2}\frac{F_n^2}{E'^2 R'}\right)^{1/3} \quad (5)$$

$$E' \cong \frac{E}{1-\nu^2}$$

A plot of the normal load versus film penetration is shown in figure 3, and curve fits of equations (4) and (5) are shown on the plot. From these curve fits an elastic modulus E for the foundation model (equation (1)) and a Hertzian contact model (equation (5)) are selected (for both models $\nu = 0.45$ is used in the curve fitting). It is noteworthy that the elastic modulus for the foundation model was found to be 260 kPa and the manufacturer reported modulus is 255 kPa.

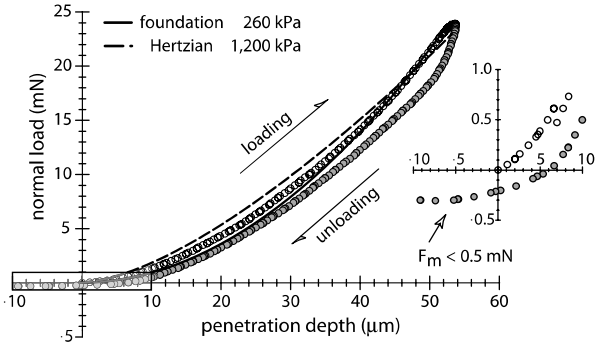

Figure 3. Experimental data collected by performing an indentation test with the microtribometer on a hydrogel contact lens. The curve fits using the modified Winkler foundation model and the Hertzian contact model are shown. The graph to the right shows a small meniscus force during unloading.

In figure 2, a schematic for a sphere sliding across the modified elastic foundation with viscous damping is shown. The deformation δ under the sphere of radius R is given in polar coordinates by equation (7). The rate of change of the deformation under the sphere is given by equation (8), where V is the sliding speed.

$$\delta = d - R + \sqrt{R^2 - r^2} \quad (7)$$

$$\dot{\delta} = \frac{r\cos(\theta)V}{\sqrt{R^2 - r^2}} \quad (8)$$

Combining equations (4), (7) and (8) gives a compact expression for the pressure distribution under a moving sphere, which is given by equation (9). Because of the (θ) term in the viscous damping portion of the foundation model, the contribution of this additional term to the integrated pressure distribution is zero (i.e. the contact area remains constant for any sliding speed and thus equation (2) holds for all sliding speeds that do not create negative pressures under the contact).

$$P_{r,\theta} = \left[\sqrt{R^2 - r^2} - \sqrt{R^2 - b^2}\right]k_s + \left[\frac{r\cos(\theta)V}{\sqrt{R^2 - r^2}}\right]\beta \quad (9)$$

Using the substitution $r = R\sin(\phi)$ the pressure distribution acting normal to the glass sphere is given by equation (10). The contact zone is over the range of angular coordinate ϕ from $\phi = 0$ to ϕ_{max}, which is given in equation (11).

$$P_{\phi,\theta} = [R(\cos(\phi) - \cos(\phi_{max}))]k_s + [\cos(\theta)\tan(\phi)V]\beta \quad (10)$$

$$\phi_{max} = \sin^{-1}\left(\frac{b}{R}\right) \quad (11)$$

The differential friction force, df_{ve}, is the projection of the normal pressure on the sphere opposing the direction of motion multiplied by the differential area, which is given in equation (12).

$$df_{ve} = P_{\phi,\theta}\sin(\phi)\cos(\theta)\, dA \quad (12)$$

The asymmetric pressure distribution (equation (10)) of the viscoelastic foundation model results in a net friction force f_{ve} for this contact geometry. The integral for the viscoelastic contribution to friction force is given by equation (13), and the solution to this integral is given by equation (14), where the dimensionless normal load F_n^* is given by equation (15).

$$f_{ve} = \int_0^{2\pi}\int_0^{\phi\,max} P_{\phi,\theta} R^2 \sin^2(\phi)\cos(\theta) d\phi\, d\theta \quad (13)$$

$$f_{ve} = \pi\beta V R^2 \left[\ln(3) - \frac{1}{2}\ln\left(9 - 6^{3/2} F_n^{*1/2}\right) - \left(\frac{2}{3}\right)^{1/2} (F_n^*)^{1/2} \right] \tag{14}$$

$$F_n^* = \frac{3F_n}{2\pi R^3 k_s} \tag{15}$$

The viscoelastic contribution f_{ve} to the friction force F_f is only one component. Two other likely contributors to the friction force are an interfacial shear stress between the asperities of the glass sphere and the contact lens f_s and the viscous shearing of a fluid film within the contact f_v. This summation of terms is given by equation (16).

$$F_f = f_{ve} + f_s + f_v \tag{16}$$

The frictional force resulting from the shearing of asperities within the contact zone f_s is described by equation (17), which assumes an interfacial shear stress τ_s acts within the apparent area of contact A that is given by equation (18).

$$f_s = \tau_s A \tag{17}$$

$$A = 2\pi\sqrt{\frac{F_n R'}{\pi k_s}} \tag{18}$$

The viscous shearing force of the fluid film within the contact zone is estimated from equation (19), which assumes a Couette flow of the trapped fluid under the contact with a viscosity η_0 and an average film thickness h. Following traditional elasto-hydrodynamic lubrication theory, it is further assumed that the film thickness can be well approximated by expressions for the minimum film thickness in soft-elasto-hydrodynamic lubrication given by equation (20) [11].

$$f_v = \eta_0 \frac{V}{h} A \tag{19}$$

$$h \cong h_{min} = 2.8 R'^{0.77} (\eta_0 V)^{0.65} E'^{-0.44} F_n^{-0.21} \tag{20}$$

Combining equations (19) and (20) give an expression for the viscous shearing contribution to the friction force f_v, which is given by equation (21). In this expression the effective elastic modulus E' is given by equation (22).

$$f_v = 1.266 (\eta_0 V)^{0.35} E'^{0.44} F_n^{0.71} R'^{-0.27} k_s^{-0.5} \tag{21}$$

$$E' = 2\frac{E}{1 - \nu^2} \tag{22}$$

The viscosity for the packing solution used in this study is reported to be $\eta_0 = 0.002$ Pa s, and the geometric variables are known, as are the sliding speed and normal load. Finally, using the results from the curve fitting of the Hertzian contact model performed in figure 3 all of the terms on the right-hand-side of equation (21) are known and can be evaluated for these experimental conditions.

The reported friction coefficient from the tribometer is a ratio of the sum of all of the friction forces divided by the applied normal load as given by equation (23).

$$\mu = (f_{ve} + f_v + f_s / F_n) \tag{23}$$

As shown in figure 3, a meniscus force can be observed during unloading in contact experiments. This force was found to be on the order of 0.5 mN, and in all subsequent curve fitting activities the meniscus force was treated as a constant. Therefore, the actual normal load was assumed to be the sum of the applied normal load and this meniscus force.

4. Results and discussion

A typical position dependent friction plot is shown in figure 4(a). The first cycle data stands apart from the others because the testing begins with no tangential strain in the flexure. The linear portion of the graph that plots friction coefficient versus lens position is related to the ratio of the tangential and normal stiffnesses of the cantilever and is a result of the sphere moving without slip along with the lens during direction reversals. The curvatures in plot of friction coefficient cannot be explained by positional changes in the normal load, which is shown in figure 4(b), or curvature of the lens. The increases in friction coefficient with time are believed to be a result of the lens drying out during testing as opposed to irreversible damage to the contact lens. Nearly identical initial values of friction coefficient on the same hydrogel lens were obtained in different tests where the lens was allowed to rehydrate in the packaging solution between tests. To further test this hypothesis the drying rate was increase by forcing dry argon across the interface; the friction coefficient increased rapidly during the intervals of argon flow.

Figure 5(a) plots the average values of friction force, excluding the reversal zones, from cycles 2–10 for 14 different experimental tests. Each data point is from a single contact lens sample and a new contact lens was used for each test. The loads varied from 10 to 50 mN and the sliding speeds varied from 63 to 6280 μm/s. Based on figure 3, estimates of the contact pressure range for this study is believed to be from 54 to 120 kPa. These pressures are an order of magnitude higher than the estimates of contact pressure experienced in the eye and the speeds are an order of magnitude lower. This range of contact pressure and load are near the limits of operation for the reciprocating microtribometer used in this study, and decreasing contact pressure and increasing reciprocating speed are left for future work. The general trend in this data is that friction force

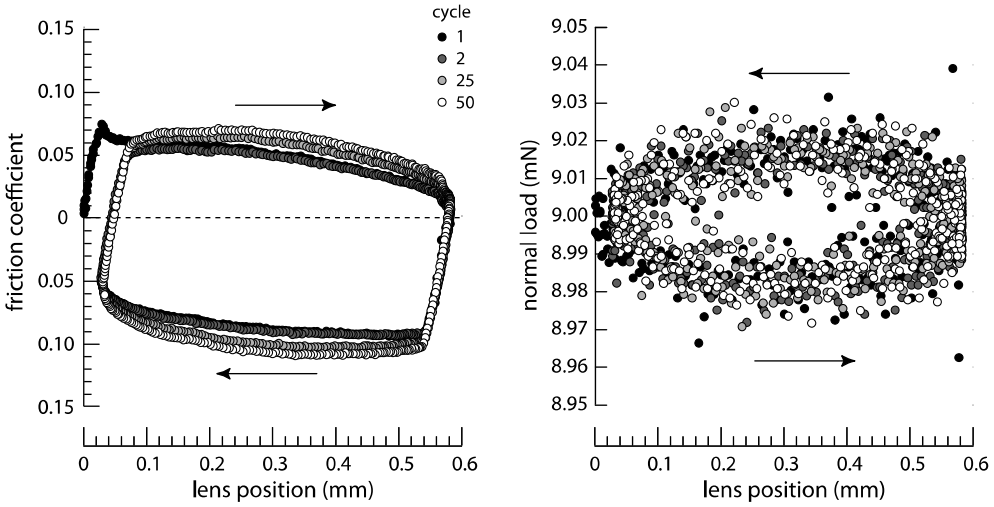

Figure 4. (a) Reported friction coefficient versus cycle number and contact lens position. The arrows denote sliding direction of the contact lens. (b) Measured normal load for the same tests. The experimental conditions were $V = 100$ μm/s and the normal load was 9 mN. The maximum variation in normal load is less than 0.5%.

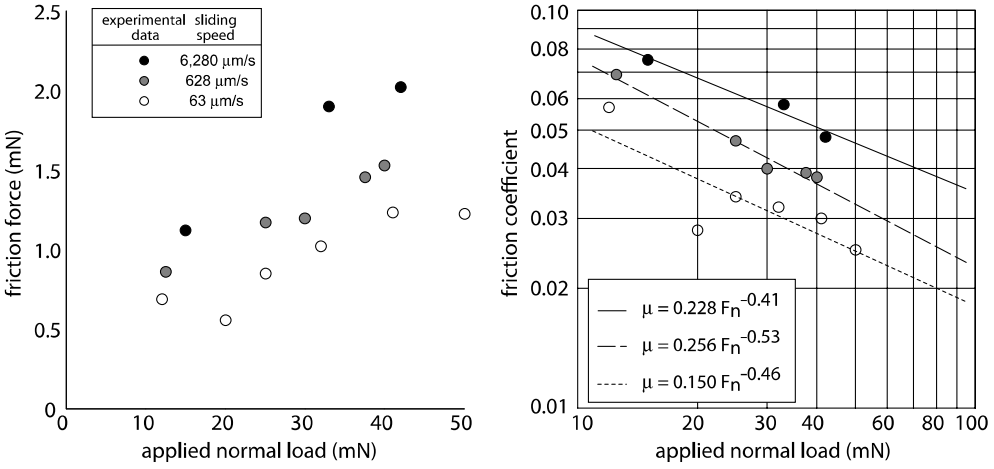

Figure 5. (a) Friction force for 14 tests varying normal load and sliding speed plotted versus normal load. (b) Reported friction coefficient versus applied normal load on a log–log plot with power-law curve fits.

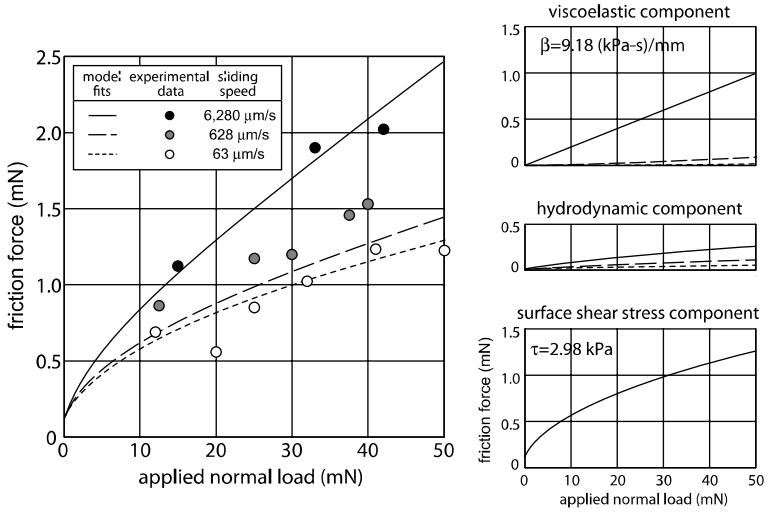

Figure 6. Comparison of the experimental data plotted in figure 5 to the curve fit model of equation (16), where the two free parameters are the viscous dissipation coefficient β, and interfacial shear stress τ_s. The values of these curve-fit parameters and the contributions of each term are shown in the graphs to the right.

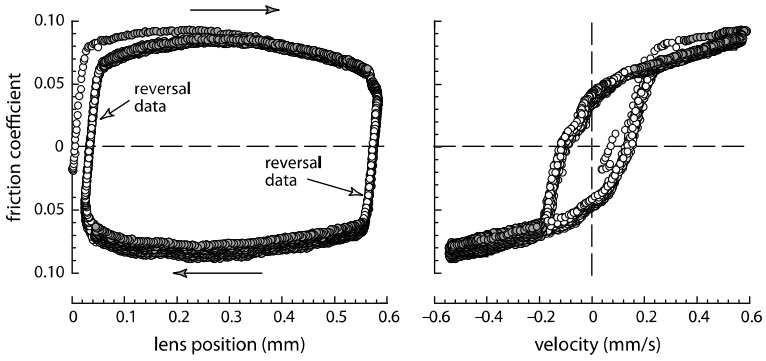

Figure 7. (a) Reported friction coefficient versus sample position for tests run on a flat hydrogel surface under 9 mN of applied normal load. The friction force data is plotted versus sliding speed in (b). The data collected during reversals is denoted by white circles, and 7 complete cycles are plotted.

increases with increasing normal load and increasing sliding speed. In figure 5(b) the reported friction coefficient is plotted versus the applied normal load on a log–log plot. The power law dependence with normal load to the −0.4 to −0.5 power is expected based on equation (23), which suggest that the dependence should be between −0.3 and −0.5.

In figure 6 the experimental data is curve fit to equation (23) with two free parameters: (1) the viscous dissipation coefficient β, and (2) the interfacial shear stress τ_s. The fits are not excellent although they do capture the trends in the experimental data. The contribution of each of the three components of the friction force (viscoelastic, hydrodynamic, and surface shear stress) are shown to the right of the plot. The viscoelastic deformation and the surface shear stress make up the majority of the friction force, with the hydrodynamic contribution representing about 10% of the total. It is of note that the calculated film thicknesses using equation (20) were between 1 and 30 nm over the entire experimental range, which suggests that the contact is in boundary lubrication not full elastohydrodynamic lubrication.

The curvature in positional friction coefficient data was puzzling until tests were run on specially prepared flat hydrogels of the same Etafilcon-A material. Figure 7(a) shows all the data from a test on one of these samples (7 cycles were run), and the maximum in friction coefficient with central track position is again visible. Following the hypothesis of a velocity dependent friction coefficient, this same data is plotted versus reciprocating speed and the linear slope of friction force with reciprocating speed for the non-reversal zone data is apparent (figure 7(b)). Additionally, the slopes do not go through 0, which is another indication that the contact is not in full hydrodynamic lubrication.

5. Conclusion

Friction tests were run on commercially available contact lenses under a range of contact pressures and speeds. The friction forces were found to be comprised of 3 components: viscoelastic dissipation, interfacial shear, and viscous shearing. A model to account for each of these contributions was developed and fit to the experimental data. This curve fitting exercise suggested that the majority of the frictional forces were due to the viscoelastic dissipation of the contact lens material and interfacial shear within the contact.

Acknowledgments

The authors gratefully acknowledge the support for Miss Rennie from the University of Florida Undergraduate Scholars Program and the support for Mrs. Dickrell from the University of Florida Minority Fellowship. Additionally financial support from Vistakon and helpful conversations with Dr. Jim Jen and Mr. Rangi Raga are greatly appreciated.

References

[1] D.K. Martin and B.A. Holden, Phys. Med. Biol. 31 (1986) 635.
[2] C.W. McCutchen, Wear 5 (1962) 1.
[3] J.A. Nairn and T. Jiangizaire (1995), ANTEC '95 3384.
[4] M.E. Freeman, M.J. Furey, B.J. Love and J.M. Hampton, Wear 241 (2000) 129.
[5] G. Hung, F. Hsu and L. Stark, Am. J. Optometr. Physiol. Optics 54 (1977) 678.
[6] M.D. Pascovici and T. Cicone, Tribol. Int. 36 (2003) 791.
[7] H.W. Liu and B. Bhushan, J. Vacuum Sci. Technol. A 21 (2003) 1528.
[8] M.D.P. Willcox, N. Harmis, B.A. Cowell, T. Williams and B.A. Holden, Biomaterials 22 (2001) 3235.
[9] P. Podra and S. Andersson, Wear 207 (1997) 79.
[10] J. Halling, T.L. Whomes, P.B. Davies and R.D. Arnell, *Tribology: Principles and Design Applications* (Springer Verlag, 1993).
[11] B.J. Hamrock and D. Dowson, J. Lubricat. Technol.—Trans. Asme 100 (1978) 236.
[12] S.H. Kim, A. Opdahl, C. Marmo and G.A. Somorjai, Biomaterials 23 (2002) 1657.